International Congress of Theoretical and Applied Mechanics 2012
August 19-24, 2012, Beijing, China

FLAT-PLATE BOUNDARY LAYER WITH CONTINUOUS FREESTREAM TURBULENCE: A PRELIMINARY DIRECT NUMERICAL SIMULATION STUDY

Xiaohua Wu
Department of Mechanical and Aerospace Engineering
Royal Military College of Canada
Kingston, Ontario, Canada K7K 7B4

Parviz Moin
Center for Turbulence Research
Stanford University
Stanford, California, U.S.A.

Abstract— We report our most recent very-large-scale direct numerical simulations (VLS DNS) with over one billion mesh points on a set of three zero pressure-gradient, smooth, incompressible, flat-plate boundary layers (ZPGFPBL). The boundary layers are beneath a continuous flow of freestream grid turbulence whose inlet strength is varied systematically from 3% (weak), 1.3% (very-weak) to 0.01% (infinitesimal) of the mean velocity. The momentum-thickness Reynolds number develops continuously starting from 80 (an exact laminar Blasius layer) at the inlet of the computational domain; and it grows to 2000 (fully turbulent) in the 3% weak perturbation case. The very-weak disturbance layer is still transitional by the exit of the computational domain, whereas the infinitesimally disturbed boundary layer remains essentially Blasius throughout. The companion thermal boundary layer is also simulated at unit molecular Prandtl number for all the three cases.

Keywords - boundary layer; direct numerical simulation.

I. INTRODUCTION

A standard boundary layer is a ZPGFPBL with infinitesimal disturbances in the sense of Schubauer and Skramstad (1947). A quasi-standard boundary layer is a nominally ZPGFPBL with finite but weak free-stream or other types of imposed perturbations (Wu 2010). They are the fundamental component of aeronautical fluid mechanics. As such, scientists and engineers are interested in the kinematics and dynamics of organized, large-scale vortex structures in the ZPGFBPL. See Head and Bandyopadhyay (1981), Kline et al (1967), Rao et al (1971), Blackwelder and Kaplan (1976), Falco (1977), Brown and Thomas (1977), Praturi and Brodkey (1978), among many others. These early landmark experimental visualization results were summarized in Cantwell (1981), Hussain (1983), Robinson (1991). More recent experimental work on the ZPGFPBL structure relies upon planar PIV technique: Adrian et al (2000), Ganapathisubramani et al (2003), Hutchins and Marusic (2007), among many others. These were summarized in Smith et al (1991), Adrian (2007), Wallace (2009). One recent remarkable low-Reynolds number flow visualization study on the ZPGFPBL was published by Delo, Kelso and Smits (2004) who demonstrated a strong agreement with the earlier work of Praturi and Brodkey (1978). Although the focus of many recent ZPGFPBL studies is on the existence and mechanism of very-large-sale motion (VLSM), e.g., Marusic et al (2010), we are of the opinion that the more basic question regarding the kinematics and dynamics of large-scale motion (LSM) in the ZPGFPBL has not been fully understood. Recent DNS studies on the ZPGFPBL are reported by Schlatter et al (2009), Lee and Sung (2011), Araya et al (2011).

The flow of flat-plate boundary layer under freestream turbulence has traditionally been tackled in the literature by considering separately the following two issues: bypass transition induced by freestream turbulence, and turbulent boundary layer beneath freestream turbulence. Boundary layer bypass transition was studied by Westin et al (1994), Matsubara and Alfredsson (2001), Jacobs and Durbin (2001), Brandt and Henningson (2002), Bake et al (200), Fransson et al (2005), Schlatter et al (2008), Ovchinnikov et al (2008). Most of these studies emphasize the role of low-momentum streaks. The streaks are considered as the result of primary instability, and the secondary instability of the streaks are viewed as the key element in breakdown. Many DNS authors used artificially manufactured fields for generating their inlet free-stream isotropic turbulence through summation of a spectrum of Fourier modes. Previous experimental studies on turbulent boundary layer under freestream turbulence focused on topics such as length scales, skin friction and conditional sampling. See Charnay et al (1976), Hunt and Graham (1978), Blair (1983), Hancock and Bradshaw (1983, 1989), Bandyopadhyay (1992), Thold and Bogard (1996). One very recent investigation along this line of attack is from Sharp, Neuscamman and Warhaft (2009).

A unique aspect of the present VLS DNS approach is its fidelity to the natural development stages of boundary layer under freestream disturbance found in turbomachinery and other aeronautical applications. There, the blade/airfoil boundary layer grows from laminar, through transition to turbulent. Our simulation approach captures such natural progression of the boundary layer development, which is contrasted to other artificial approaches relying upon periodicity/recycling in which transitional boundary layer and turbulent boundary layer are computed separately in two flows. The current VLS DNS design with continuous freestream turbulence also removes the discrete and intermittent perturbation character adopted in our previously reported simulations (Wu and Moin 2009a,b, 2010; Wu 2010).

II. GENERATION OF INFLOW TURBULENCE

All the computational aspects of the present boundary layer DNS including domain size, details of the grid and time stepping are identical to that of Wu and Moin (2010), except for the continuous freestream turbulence.

The continuous inflow stream was generated by stitching together 25 independent, temporally decaying blocks of homogeneous isotropic turbulence. These temporally decaying grid turbulence simulations were performed separately using a completely different numerical method from that used for the main boundary layer DNS. For the generation of grid turbulence, the time-dependent, compressible Navier-Stokes equations were solved at the incompressible limit. A second-order spatial scheme was used in which the convective and pressure terms were treated with an alternately biased stencil resulting in a centered finite-difference approximation over one time-step. The diffusive terms were solved using a centered stencil whereas the time was advanced using a second-order Runge-Kutta scheme at a fixed time step. Aliasing caused by the triple non-linearity in the compressible equations was reduced by the use of skew-symmetric convective terms. In addition, great care was taken to ensure adequate resolution of small scales turbulence, which removed the requirement of explicit filtering and reduced the dispersion error of the scheme. Each of these 25 statistically independent simulations had a resolution of 256 grid points distributed in a triply periodic cubic computational domain of $2\pi L_{iso}$, where L_{iso} is the unit characteristic length scale specific to the isotropic turbulence simulation.

The approach for prescribing initial condition for the decaying isotropic turbulence follows Mansour and Wray (1994). Specifically, the isotropic grid turbulence simulations were initialized by a divergence-free velocity field with a specified initial energy spectrum and initial intensity. Randomness was then superimposed so that each of the 25 simulations started from a unique set of initial velocity fields. The initial Taylor micro-scale Reynolds number Re_λ was set at 72. The initial turbulent intensity was approximately 15%. At the instant when the grid turbulence intensity has decayed to almost exactly 3%, the instantaneous isotropic velocity fields were saved for subsequent boundary layer DNS inflow condition. This instant corresponds to a Taylor micro-scale Reynolds number Re_λ approximately 15. The corresponding longitudinal Taylor micro-scale λ is approximately $0.32\,L_{iso}$, nearly 5% of the length of the isotropic grid turbulence simulation box. A validation of the grid turbulence statistics was conducted to assure the physical nature of our inflow turbulence. It is well-accepted that the streamwise velocity derivative skewness in incompressible grid turbulence should attain a nearly constant value between -0.6 and -0.4. The computed present ensemble-averaged velocity derivative skewness remained nearly constant at the expected value -0.5 after an initial transience. The incompressibility and isotropy of the grid turbulence was further verified by investigating the two-point correlations. It was found that computed the longitudinal correlation and transverse correlation are related according to incompressible isotropic turbulence theory.

To introduce the isotropic turbulence stream into the boundary layer DNS domain, the spatial coordinates of the pre-generated isotropic turbulence cubes were first rescaled to ensure that the cube dimension in each direction $2\pi L_{iso}$ is identical to the span of the boundary layer simulation, $562.5\,\theta_0$. Here, θ_0 is the inlet boundary layer momentum thickness and the unit characteristic length scale for the boundary layer DNS. Characteristic velocity scale in the temporally decaying isotropic turbulence and that in the boundary layer DNS are both 1.0. Therefore, at the inlet plane, the freestream turbulence intensity is also 3%. To be consistent with that in Wu and Moin (2009a,b, 2010) and Wu (2010), the inlet momentum thickness Reynolds number $\mathrm{Re}_\theta = 80.$ There is a small adjustment in the length scales of the introduced isotropic turbulence near the inlet of the boundary layer simulation domain. The effect of the adjustment on the boundary layer development is presumably to be small.

The 25 cubes were then aligned and stacked sequentially forming a narrow cuboid-shaped band with a size of 14062.5 $\theta_0 \times 562.5\,\theta_0$ times $\times 562.5\,\theta_0$. At the inlet plane, the longer edge of the isotropic turbulent band is aligned with the far upstream velocity direction so that the band is transported into the computational domain by the far upstream velocity. The lower edge of the band is located $15\,\theta_0$ away from the wall at the inlet, similar to that of Wu and Moin (2009a,b, 2010). This is to ensure that the Blasius boundary layer at the inlet is undistorted by the imposed perturbations, which avoids the arbitrariness inherent in prescribing perturbed velocity profiles inside the layer. On the inlet plane, the inflow velocity field is a simple vector summation of the uniform far upstream velocity with the temporally and spatially interpolated grid turbulence stream velocity field. Because the streamwise computational domain length is x=12750 θ_0, it takes more than one flow-through time to exhaust the streamwise dimension of the grid turbulent band due to time advancement, at which point the band is simply re-used.

III. OVERALL VIEW OF THE BOUNDARY LAYER

Cross-sectional views of the velocity and thermal boundary layers over a streamwise/wall-normal xy-plane are shown in Fig.1. The velocity boundary layer in Fig.1a is shrouded by freestream fluctuation, which makes it difficult to distinguish boundary layer turbulence from freestream turbulence. The thermal boundary layer shown in Fig.1b is free from freestream fluctuations since there is no temperature fluctuation at the inlet. This provides an excellent way for discriminating the boundary layer turbulence from the freestream turbulence. Although not shown here, the 1.3% inlet FST case has minor departure from the laminar profile, and the 0.01% inlet FST case is almost exactly Blasius.

Three-dimensional, instantaneous view of the transitional boundary layer in the region is given in Fig.2 using iso-surfaces of swirling strength λ_{ci} (Adrian and Liu 2002). The iso-surfaces are colored by y/δ. The freestream turbulence structures visible in Fig.1a block views of the structures inside the boundary layer. These freestream structures are removed by choosing a higher threshold value in Fig.2. Similar view of the turbulent boundary layer over the fully-turbulent region after removal of freestream turbulence structures is given in Fig.3. The preponderance of hairpin vortices, in the form of hairpin forests, in both the transitional and turbulent boundary layers observed from the present moderate-Reynolds-number flow is very much like those reported previously in Wu and Moin (2009a,b and 2010) and in Wu (2010). The structures observed in the pipe flow of Wu and Moin (2008) with streamwise periodic boundary condition are different from the hairpin forests in Fig.2 and Fig.3.

Boundary layer integral parameters are shown in Fig.4. The velocity boundary layer thickness and the thermal boundary layer thickness are both defined using 99% of the corresponding freestream value, and they exhibit general agreement with each other. This suggests that at least for visualization purpose the thermal boundary layer (with no freestream temperature fluctuation) can be considered as a good proxy of the velocity boundary layer (shrouded by freestream fluctuation). Shape factor H follows the Blasius solution quite closely until breakdown, which is an indication that perturbations in the present DNS are well-controlled. In comparison, the T3A shape factor departs from the Blasius solution right from the beginning. Similar to our previous DNS results, Reynolds analogy holds very well in the present transitional and turbulent boundary layers as evident by fact that the ratio between twice Standon number and skin friction coefficient is nearly 1.0 throughout the streamwise domain. The molecular Prandtl number used in the DNS is 1.

Skin-friction coefficients from the primary case and the two auxiliary cases are presented in Fig.5. The results are also contrasted with our previous DNS results and with previous experimental data for turbulent and transitional boundary layers. Skin-friction coefficient in the 0.01% infinitesimal inlet freestream turbulence case behaves exactly as expected, which provides a limiting case test for the primary case. It should be noted that both the auxiliary cases were performed using the same grid as the primary case. The 1.3% inlet freestream turbulence case only shows minor departure from the Blasius solution by the exit, indicating that the flow is still in the early transitional phase. Skin-friction coefficient in the primary case, in the case of Wu and Moin (2010) with patches of freestream turbulence, and in the case of Wu (2010) with passing wakes all collapse on to the Blasius solution prior to their breakdown. They also show good agreement with previous experimental data on the turbulent boundary layer after the completion of transition. The present skin-friction coefficient is also in fair agreement with that from the T3A bypass transition experiment, suggesting that the present transitional boundary layer is a typical bypass transitional flow.

Mean and second-order turbulent statistics of the boundary layer have been thoroughly compared with classical experimental data and contrasted with those of Wu and Moin (2010) and Wu (2010). Those comparison results, though not shown here, suggest that the present simulated flow after transition is a typical turbulent boundary layer at moderate Reynolds number compatible with many past wind-tunnel experiments. The low freestream turbulence fluctuations of less than 1% can be considered negligible for structural studies on the turbulent boundary layer, as in Kline et al. (1967) and Adrian et al. (2000). The turbulent statistics also demonstrate a close agreement with those of Wu and Moin (2000). The agreement with those of Wu (2010) is only limited beneath the buffer region since the freestream passing wakes with their mean deficit in that flow impose a rather strong disturbance to the boundary layer.

ACKNOWLEDGMENT

The computer program used in this study was developed by the late Dr. Charles D. Pierce of the Center for Turbulence Research at Stanford. This work was supported by U.S. Department of Energy, NSERC Discovery Grant, Department of Defense Academic Research Program (ARP), and the Canada Research Chair Program (CRC). The inflow isotropic turbulence stream was generated by Mr. Jean-Pierre Hickey. The simulations were performed at the High Performance Computing Virtual Laboratory (HPCVL). The kind assistance from the HPCVL staff is gratefully acknowledged.

REFERENCES

[1] Schubauer, G.B. and Skramstad, H.K., 1947, "Laminar boundary layer oscillations and stability of laminar flow", J. Aero. Sci., Vol. 14, pp. 69-78.

[2] Wu, X., 2010, "Establishing the generality of three phenomena using a boundary layer with passing wakes", J. Fluid Mech., Vol. 664, pp.193-219.

[3] Head, M.R. and Bandyopadhyay, P., 1981, "New aspects of turbulent boundary layer structure", J. Fluid Mech., Vol. 107, pp. 297-338.

[4] Kline, S.J., Reynolds, W.C., Schraub, F.A. and Runstadler, P.W., 1967, "The structure of turbulent boundary layers", J. Fluid Mech., Vol. 95, pp. 741-773.

[5] Rao, K.N., Narasimha, R. and Narayanan, M.A.B., 1971, "Bursting in a turbulent boundary layer". J. Fluid Mech., Vol. 48, pp. 339-352.

[6] Blackwelder, R.F. and Kaplan, R.E., 1976, "On the wall structure of the turbulent boundary layer", J. Fluid Mech. Vol. 76, pp. 89-112.

[7] Falco, R.E., 1977, "Coherent motions in the outer region of turbulent boundary layers", Phys. Fluids, Vol. 20, pp. 5124-5132.

[8] Brown, G.L. and Thomas, A.S.W., 1977, "Large structure in a turbulent boundary layer", Phys. Fluids, Vol. 20, pp. S243-S252.

[9] Praturi, A.K. and Brodkey, R.S., 1978, "A stereoscopic visual study of coherent structures in turbulent shear flow". J. Fluid Mech., Vol. 89, pp. 251-272.

[10] Cantwell, B.J., 1981, "Organized motion in turbuelnt flow", Ann. Rev. Fluid Mech., Vol. 13, pp. 457-515.

[11] Hussain, A.K.M.F., 1983, "Coherent structures – reality and myth", Physics. Fluid, Vol. 26, pp. 2816-2850.

[12] Robinson, S.K., 1991, "Coherent motion in the turbulent boundary layer", *Ann. Rev. Fluid Mech.*, Vol. 23, pp. 601-639.

[13] Adrian, R.J., Meinhart C.D. and Tomkins, C.D., 2000, "Vortex organization in the outer region of the turbulent boundary layer", J. Fluid Mech., Vol. 422, pp. 1-54.

[14] Ganapathisubramani, B. Longmire, E.K. and Marusic, I., 2003, "Characteristics of vortex packets in turbulent boundary layers," J. Fluid Mech. Vol. 478, pp. 35.

[15] Smith, C.R., Walker, J.D.A., Haidari, A.H. and Sobrun, U., 1991, "On the dynamics of near-wall turbulence," *Philosophical Transcations Royal Society London A*, Vol. 336, pp. 131-175.

[16] Adrian, R.J., 2007, "Hairpin vortex organization in wall turbulence". *Phys. Fluids*, Vol. 19, 041301.

[17] Wallace, J.M., 2009, "Twenty years of experimental and direct numerical simulation access to the velocity gradient tensor: what have we learned about turbulence". Phys. Fluids, Vol. 21, 021301.

[18] Delo, C.J., Kelso, R.M. and Smits, A.J., 2005, "Three dimensional structure of a low Reynolds number turbulent boundary layer", J. Fluid Mech. Vol. 512, pp. 47-83.

[19] Marusic, I. McKeon, B.J., Monkewitz, P.A., Nagib, H.M., Smits, A.J. and Sreenivasan, K.R., 2010, "Wall-bounded turbulent flows at high Reynolds numbers: Recent advances and key issues", *Physics Fluid*, Vol. 22, 065103.

[20] Schlatter, P.. Örlü, R., Li, Q., Brethouwer, G., Fransson, J.H.M., Johansson, A.V., Alfredsson, P.H., Henningson, D.S., 2009, "Turbulent boundary layers up to $\mathrm{Re}_\theta = 2500$ studied through simulation and experiment", Phys. Fluids, Vol. 21, 051702.

[21] Lee, J.H. and Sung, H.J., 2011, "Very-large-scale motions in a turbulent boundary layers", J. Fluid Mech., in press.

[22] Araya, G., Castillo, L., Meneveau, C. and Jansen, K., 2011, "A dynamic multi-scale approach for turbulent inflow boundary conditions in spatially-developing flow", *J. Fluid Mech*., Vol. 670, pp. 581 – 605.

[23] Westin, K.J.A., Boiko, A.V., Klingmann, B.G.B., Kozlov, V.V. and P.H. Alfredsson, 1994, "Experiments in a boundary layer subject to freestream turbulence. Part I. Boundary layer structure and receptivity", J. Fluid Mech., Vol. 281, pp. 193-218.

[24] Matsubara, M. and Alfredsson, P.H., 2001, "Disturbance growth in boundary layers subjected to freestream turbulence", J. Fluid Mech., Vol. 430, pp. 149-168.

[25] Jacobs, R.G. and Durbin, P.A., 1998, "Shear sheltering and the continuous spectrum of the Orr-Sommerfeld equation", Phys. Fluids, Vol. 10, pp. 2006-2011.

[26] Brandt, L. and Henningson, D.S., 2002, "Transition of streamwise streaks in zero-pressure-gradient boundary layers", J. Fluid Mech., Vol. 472, pp. 229-261.

[27] Bake, S., Meyer, D.G. and Rist, U., 2002, "Turbulence mechanism in Klebanoff transition: a quantitative comparison of experiment and direct numerical simulation, J. Fluid Mech., Vol. 459, pp. 217-243.

[28] Fransson, J.H.M., Matsubara, M. and Alfredsson, P.H., 2005, "Transition induced by freestream turbulence", J. Fluid Mech., Vol. 527, pp. 1-25.

[29] Schlatter, P., Brandt, L., de Lange, H.C. and Henningson, D.S., 2008, "On streak breakdown in bypass transition", Phys. Fluids, Vol.20, 101505.

[30] Ovchinnikov, V., Choudhari, M.M. and Piomelli, U., 2008, "Numerical simulations of boundary-layer bypass transition due to high-amplitude free-stream turbulence", J. Fluid Mech., Vol. 613, pp. 135-169.

[31] Hancock, P.E. and Bradshaw, P., 1989, "Turbulence structure of a boundary layer beneath a turbulent freestream", J. Fluid Mech., Vol. 205, pp. 45-76.

[32] Sharp, N.S., Neuscamman, S. and Warhaft, Z., 2009, "Effects of large-scale freestream turbulence on a turbulent boundary layer", Phys. Fluids, Vol. 21, 095105.

[33] Wu, X. and Moin, P., 2008, "A direct numerical simulation study on the mean velocity characteristics in turbulent pipe flow", J. Fluid Mech., Vol. 608, 81-112.

[34] Wu, X. and Moin, P., 2009a, "Direct numerical simulation of turbulence in a nominally-zero-pressure-gradient flat-plate boundary layer", J. Fluid Mech., Vol. 630, pp. 5-41.

[35] Wu, X. and Moin, P., 2009b, "Forest of hairpins in a low-Reynolds-number zero-pressure-gradient flat-plate boundary layer", Phys. Fluids, Vol. 21, 091106.

[36] Wu, X. and Moin, P., 2010, "Transitional and turbulent boundary layer with heat transfer", Phys. Fluids, Vol. 22, 085105.

[37] Mansour, N. N. and Wray, A. A., 1994, "Decay of isotropic turbulence at low Reynolds number", Phys Fluids, Vol. 6, pp. 808-814.

[38] Adrian, R.J. and Liu, Z.C., 2002, "Observation of vortex packets in direct numerical simulation of fully turbulent channel flow", J. Visualization, Vol. 5, pp. 9-19.

[39] Purtell, L.P., Klebanoff, P.S. and Buckley, F.T., 1981, "Turbulent boundary layer at low Reynolds number", Phys. Fluids, Vol. 24, pp. 802-811.

[40] DeGraaff, D.B. and Eaton, J.K., 2000, "Reynolds-number scaling of the flat-plate turbulent boundary layer", J. Fluid Mech., Vol. 422, pp. 319-346.

[41] Roach, P.E. and Brierley, D.H., 1990, "The influence of a turbulent frees-stream on zero pressure gradient transitional boundary layer development, part I: Test Cases T3A and T3B". In Numerical Simulation of Unsteady Flows and Transition to Turbulence, pp. 319-347, Cambridge University Press.

(a)

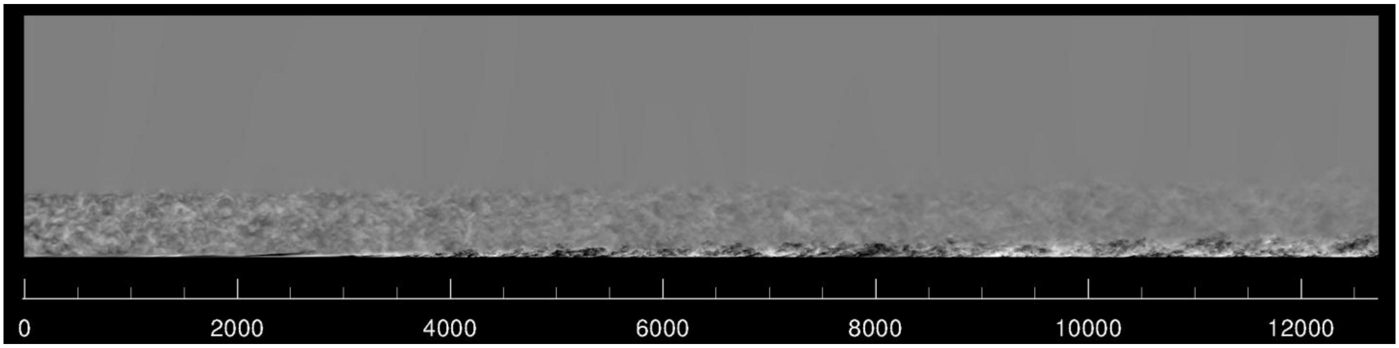

(b)

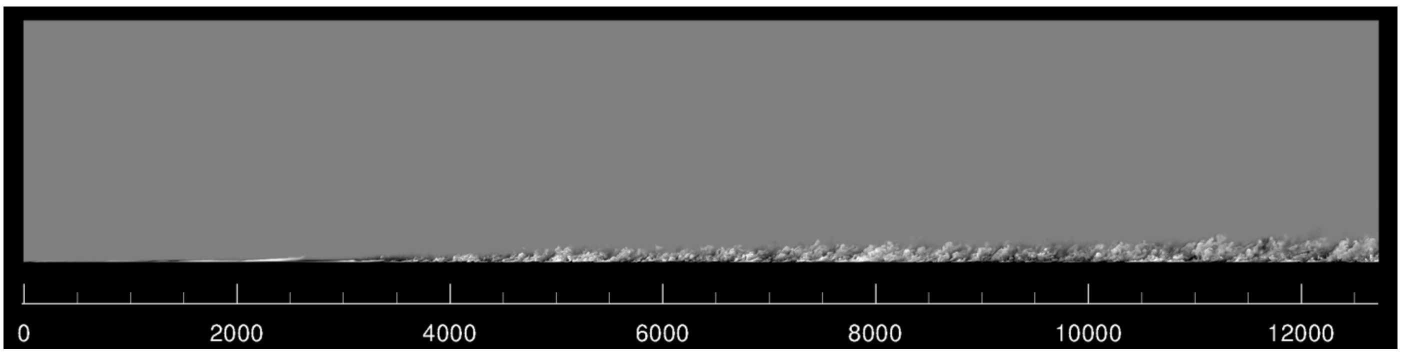

(c)

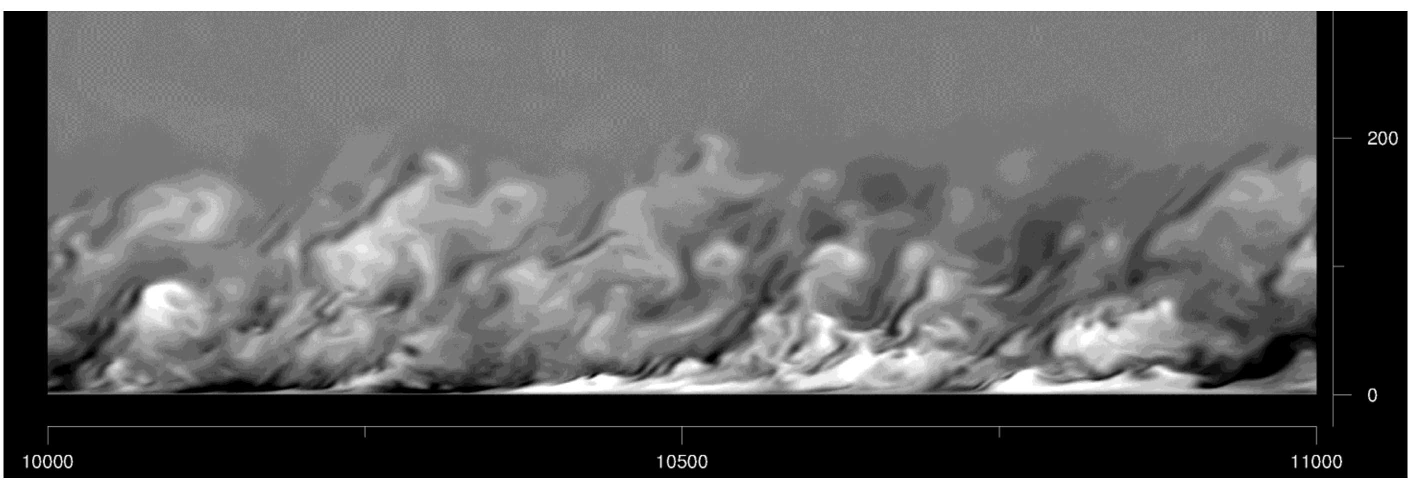

Fig.1 Cross-sectional view of the boundary layers over a random xy-plane. (a): streamwise velocity fluctuation in the primary case with 3% inflow turbulence; (b) and (c) (zoomed view): temperature fluctuation in the primary case with 3% inflow turbulence.

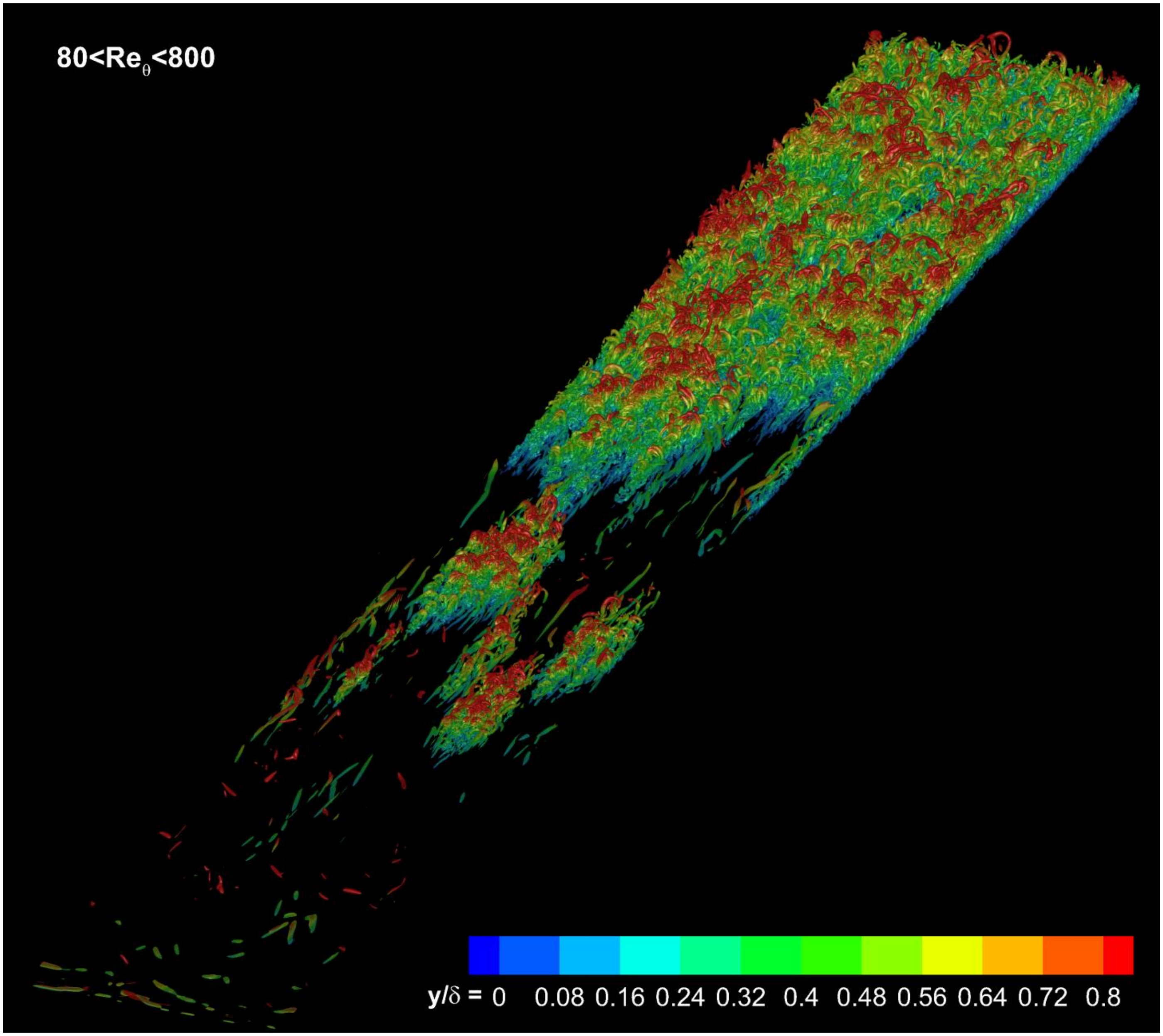

Fig.2. λ_{ci} colored colored by y/δ at a random instant in the transitional region with 3% inlet freestream turbulence.

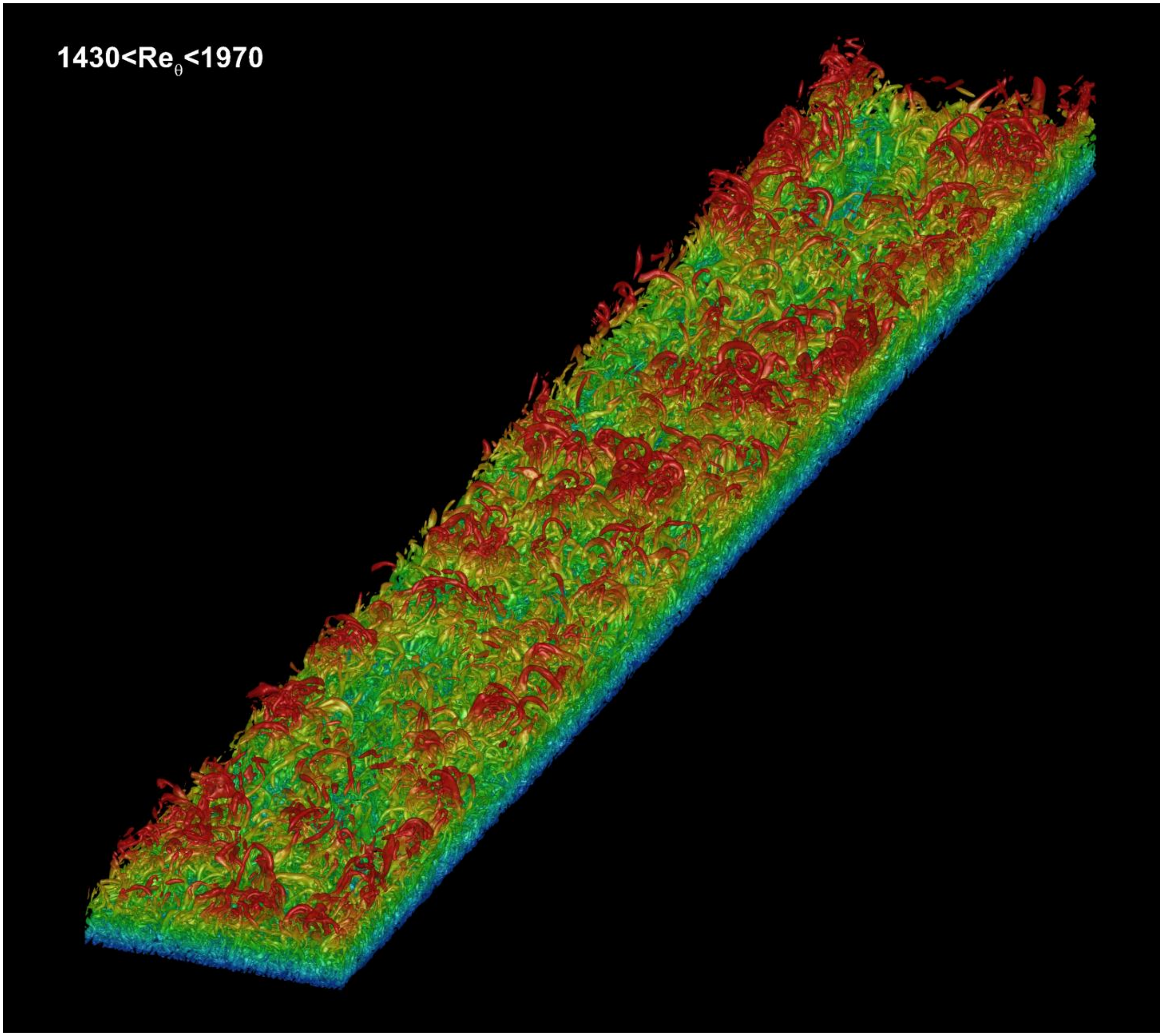

Fig.3. λ_{ci} colored colored by y/δ at a random instant in the fully-turbulent region with 3% inlet freestream turbulence.

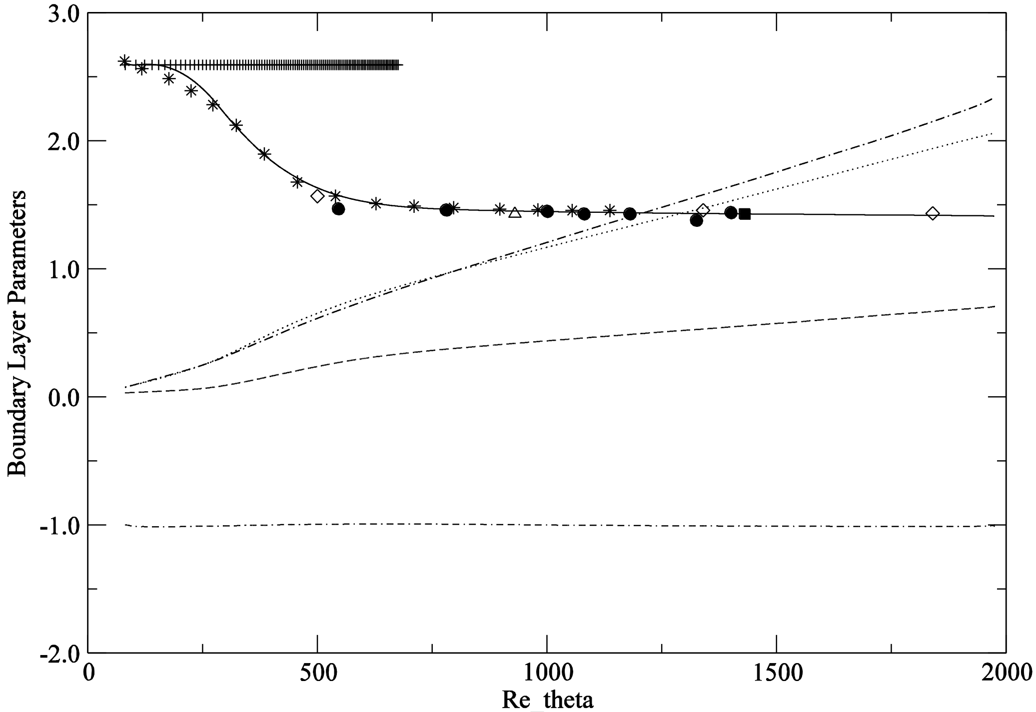

Fig.4: Boundary layer integral parameters as a function of Re_θ. Lines: present DNS; dotted: boundary layer thickness $10^{-2}\delta/\theta_0$; solid: H; dash: $10^{-3}\mathrm{Re}_\tau$; dash-dot: thermal boundary layer thickness $10^{-2}\delta_\varphi/\theta_0$; dot-dash-dash-dot: $-2St/C_f$. Cross: Blasius solutions; diamond: Purtell et al; circle: Kline et al; triangle: Adrian et al; square: DeGraaff & Eaton.

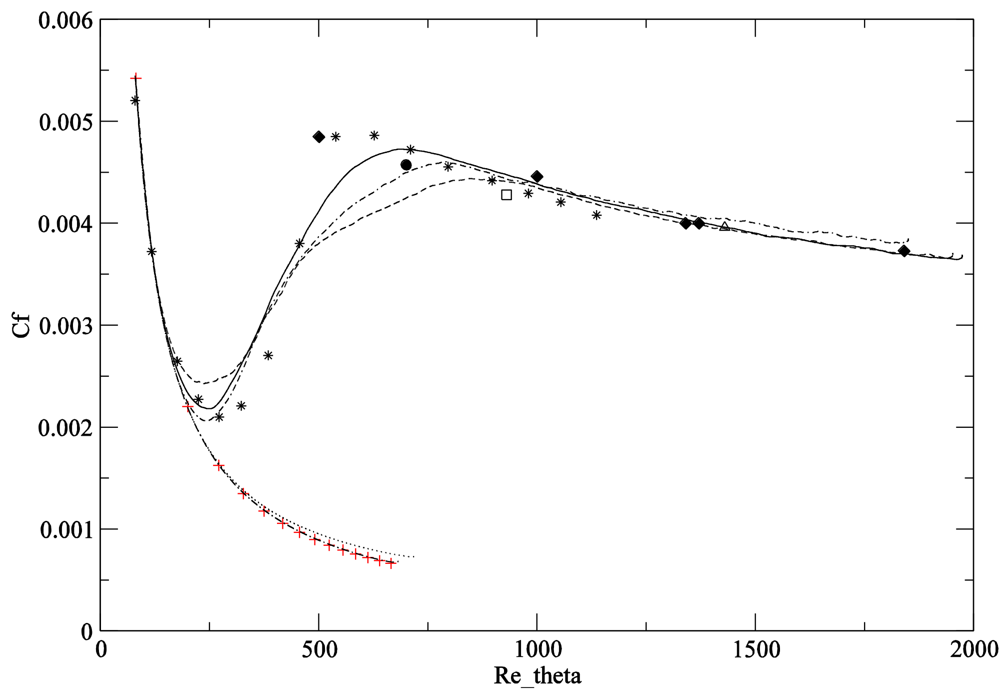

Fig.5 Variation of skin friction with Re_θ. Present DNS: solid: 3% inlet-FST case; dotted: 1.3% inlet-FST case; dash-dot-dash: 0.01% inlet-FST case. Previous DNS: dashed: Wu and Moin (2009) with freestream blocks of turbulence; dot-dash-dash-dot: Wu (2010) with freestream wakes. Experimental data: diamond: Purtell et al; box: Adrian et al; triangle-up: DeGraaff and Eaton; circle: Del, Kelso and Smits; star: T3A of Roach and Brierly (1990); plus: Blasius solution.